NANO MICRO small

Supporting Information

for *Small,* DOI: 10.1002/smll.202005179

Acoustofluidics-Assisted Fluorescence-SERS Bimodal Biosensors

*Nanjing Hao, Zhichao Pei, Pengzhan Liu, Hunter Bachman, Ty Downing Naquin, Peiran Zhang, Jinxin Zhang, Liang Shen, Shujie Yang, Kaichun Yang, Shuaiguo Zhao, and Tony Jun Huang**

Supporting Information

Acoustofluidics-Assisted Fluorescence-SERS Bimodal Biosensors

*Nanjing Hao, Zhichao Pei, Pengzhan Liu, Hunter Bachman, Ty Downing Naquin, Peiran Zhang, Jinxin Zhang, Liang Shen, Shujie Yang, Kaichun Yang, Shuaiguo Zhao, and Tony Jun Huang**

Optimization process of device parameters: In our recent studies, we examined the effect of the acoustofluidic sharp-edge mixer structures in mixing performance through experimental investigations[1–3] and theoretical simulations.[4,5] Generally, 1) number of sharp-edges: Increasing the number of sharp-edges can permit intensive mixing of fluids.[2] However, it is not necessary to continuously increase the sharp-edges when the complete mixing is achieved. 2) tip angle of sharp-edges: The smaller the tip angle of sharp-edges, the larger the vibration amplitude and thus the stronger the acoustic streaming effects for intensive mixing.[1] 3) distance between two adjacent sharp-edges: Increasing the distance between two adjacent sharp-edges to 2 times and above (>600 μm) does not favor the generation of eddies near the tips, suggesting undesirable mixing performance.[5] 4) width of PDMS microchannel (W) and height of sharp-edges (H): Increasing the ratio of W/H can break the flow pattern into two distinct vortices and eddies might not be present at high values of W/H, which means that expanding the width of microchannel or contracting the height of sharp-edge structures is not desirable for achieving complete mixing.[4,5]

Operating conditions (Applied voltage, frequency, and flow rate): For the synthesis of 3D ZnO-Ag plasmonic nanoarray, the acoustic transducer (PUI Audio, AB2720B-LW100-R) was driven with an applied voltage and frequency of 10 V and 4.25 kHz, respectively. According to our experimental investigations and previous studies,[1,3] a higher applied voltage (> 10 V) can generate faster mixing performance inside the acoustofluidic sharp-edge device, but it is not necessary since the applied voltage at 10 V is enough to permit complete mixing. Whereas, lower voltage at 5 V or below cannot permit intensive mixing of reactants, and the inefficient mixing may lead to uneven nanoarray pattern inside glass capillary. Regarding the applied frequency, the strongest acoustic streaming effect is generated at around 4.0 kHz. The device performance variation is usually observed from batch to batch due to the manufacturing process and PDMS material/substrate used). In addition, flow rate plays a significant role in the uniformity of 3D plasmonic nanoarray. Higher flow rates can generate more uniform nanorod array from the entrance to the exit of square-shaped glass capillary, but it is at the expense of greater reactants consumption. Whereas, lower flow rates can lead to more obvious gradient length distribution profiles from the entrance to the exit of glass capillary.

Estimation of homogeneous mixing time in acoustofluidic sharp-edge mixer: Herein, the width and depth of the PDMS microchannel are 600 μm and 50 μm, respectively. Each sharp-edge has a constant height of 300 μm, and the distance between two adjacent sharp-edges is 300 μm. To estimate the complete mixing time, we observed that two fluids can be completely mixed after only passing through the first two sharp-edge structures when injecting both fluids at a flow rate of 1 μL/min. Therefore, the mixing distance is estimated to be less than 1,000 μm. Without the consideration of the volume of sharp-edge structures, the corresponding complete mixing time is estimated to be 0.9 s; when considering it, the complete mixing time should be even less.

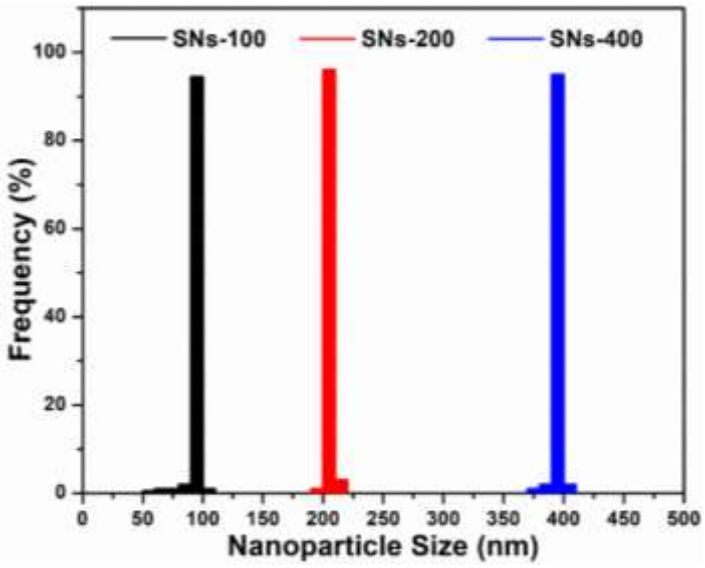

Figure S1: Statistical size distributions of silica nanoparticles from 200 particles under SEM.

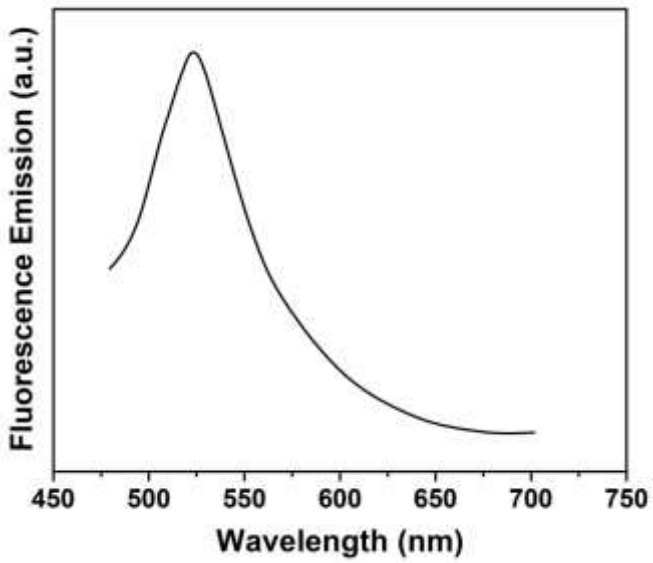

Figure S2: Fluorescence emission spectrum of fluorescent exosome standard (Excitation at 450 nm). See more information from Biovision Incorporated (https://www.biovision.com/documentation/datasheets/M1075.pdf)

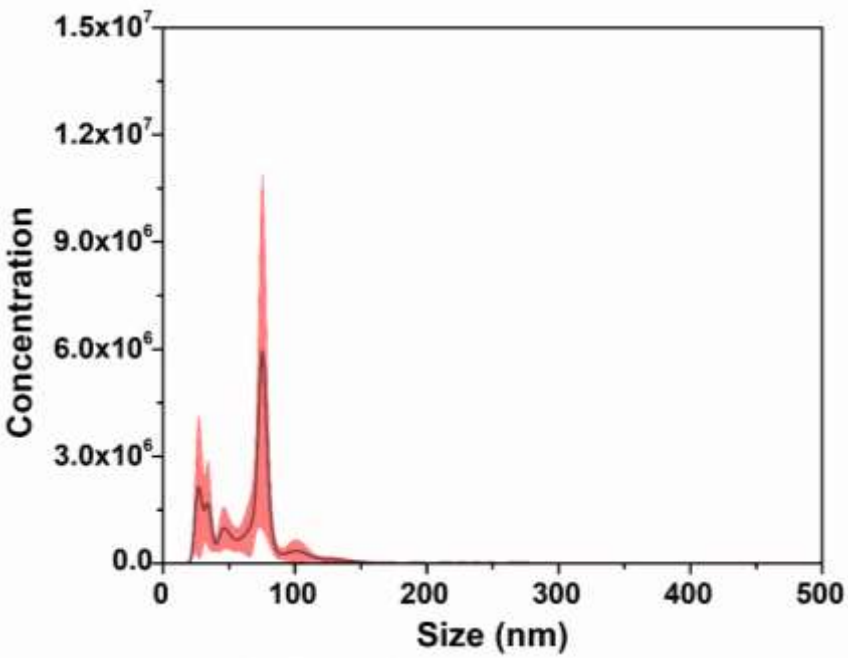

Figure S3: NTA analysis showing the size distribution profiles of ExoStd™ human urine fluorescent exosomes.

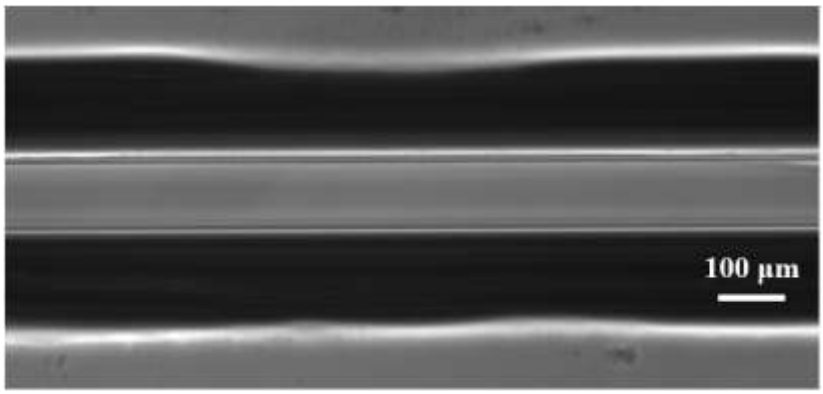

Figure S4: Top view optical image of solution with exosome-bound SNs-400 when the SAW was OFF.

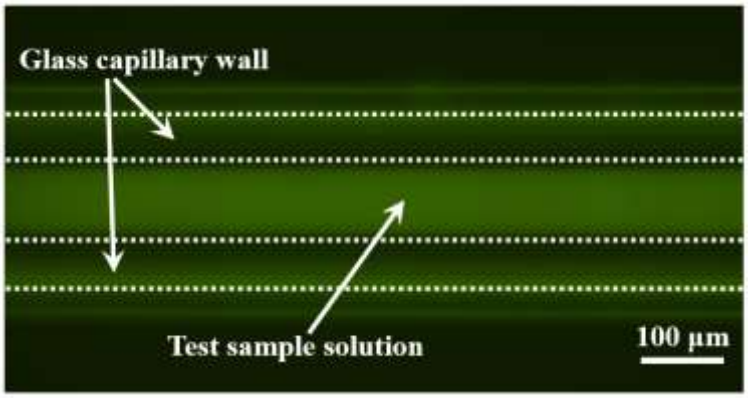

Figure S5: Top view microscope image of solution with exosome-bound SNs-400 when excited by the fluorescent light (~488 nm) under acoustic OFF status. The exposure time was increased from 100 ms to 1 s for better observation.

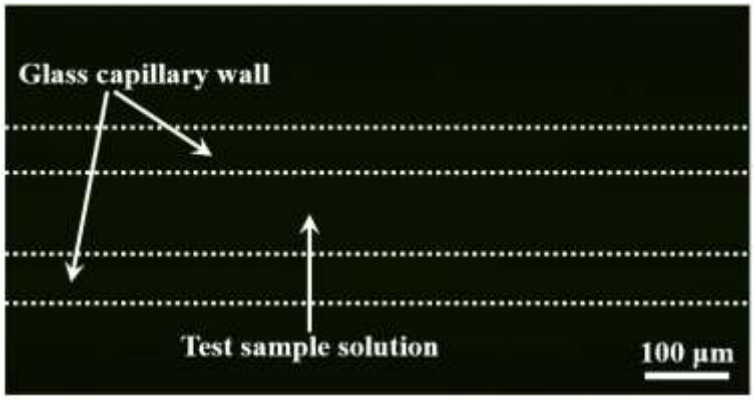

Figure S6: Top view microscope image of PBS solution with SNs-400 when excited by the fluorescent light (~488 nm). The exposure time was 100 ms.

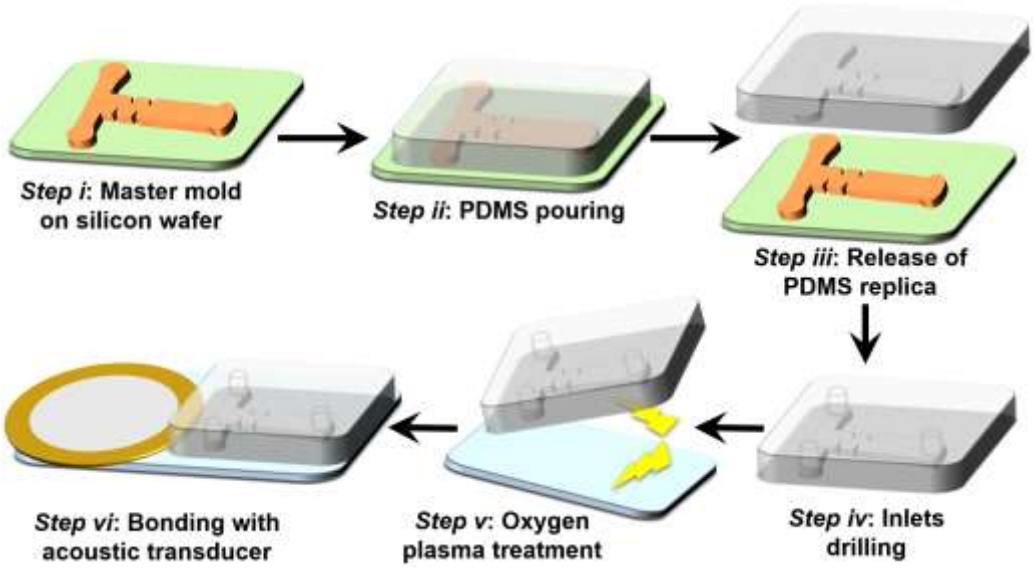

Figure S7: Schematic diagram showing the fabrication workflow of acoustofluidic sharp-edge mixer.

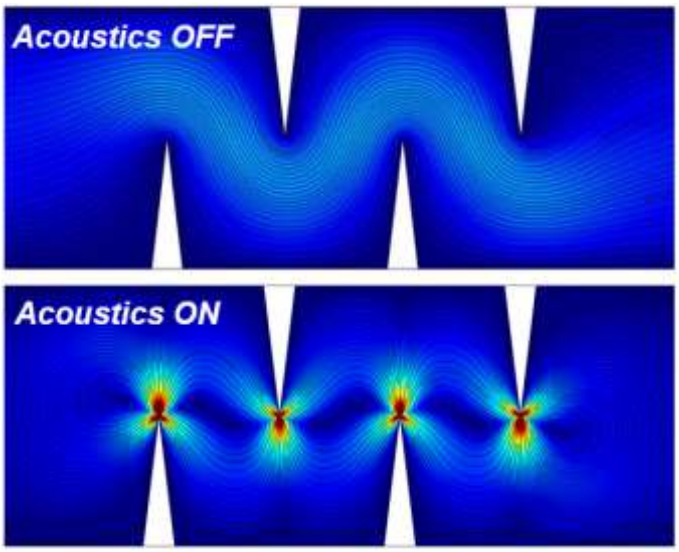

Figure S8: Simulation of acoustic streaming patterns.

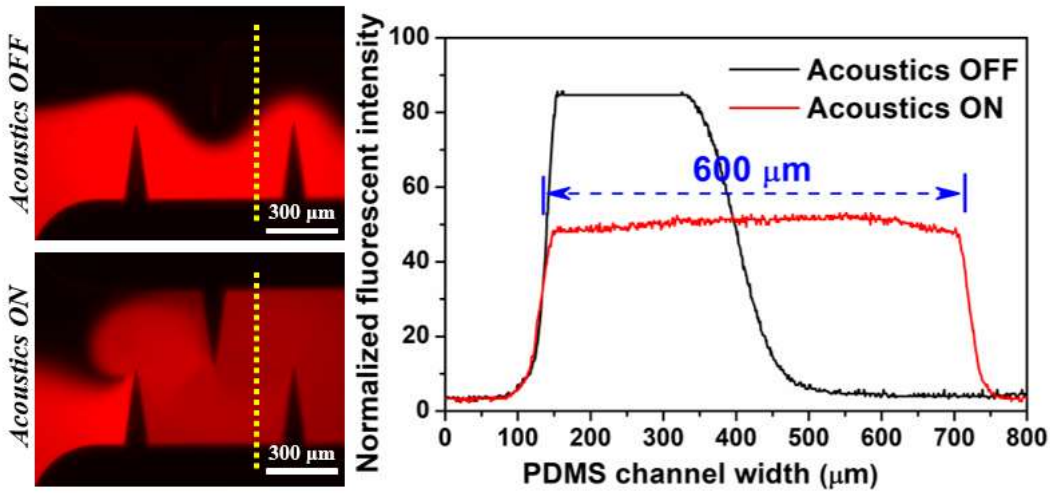

Figure S9: Normalized fluorescent distribution profiles across the microchannel width of acoustofluidic sharp-edge mixer from the yellow dash lines (analyzed from bottom to up direction). Results were obtained with an applied voltage, frequency, and flow rate of 10 V, 4.25 kHz, and 1 μL/min, respectively.

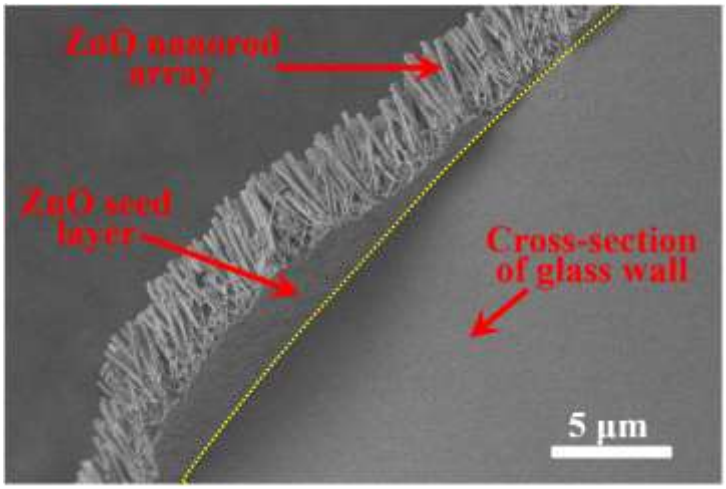

Figure S10: SEM image showing the fine structures of ZnO nanoarray inside square-shaped glass capillary. The glass capillary was broken into pieces before characterization, and the yellow line is the boundary between glass wall and ZnO materials.

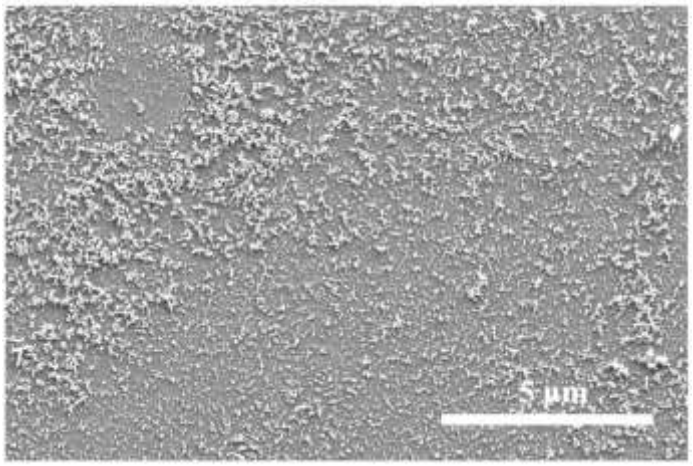

Figure S11: SEM image of the resultant ZnO materials in the absence of acoustics (Acoustics OFF).

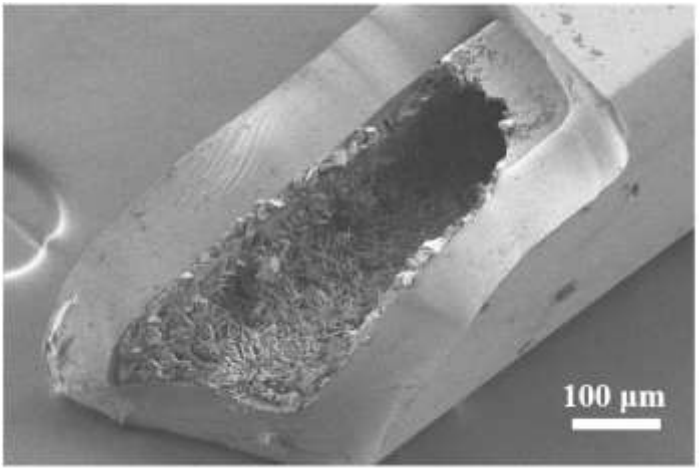

Figure S12: SEM image of the resultant ZnO materials when continuously operating for 5 hours during the growth step.

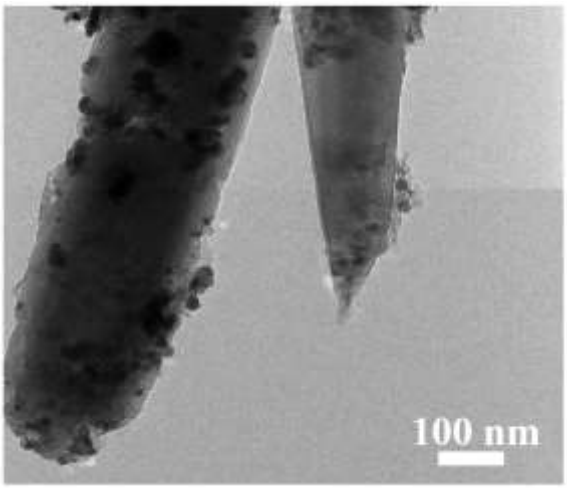

Figure S13: TEM image of ZnO-Ag sample that was scratched from the inner wall of square-shaped glass capillary.

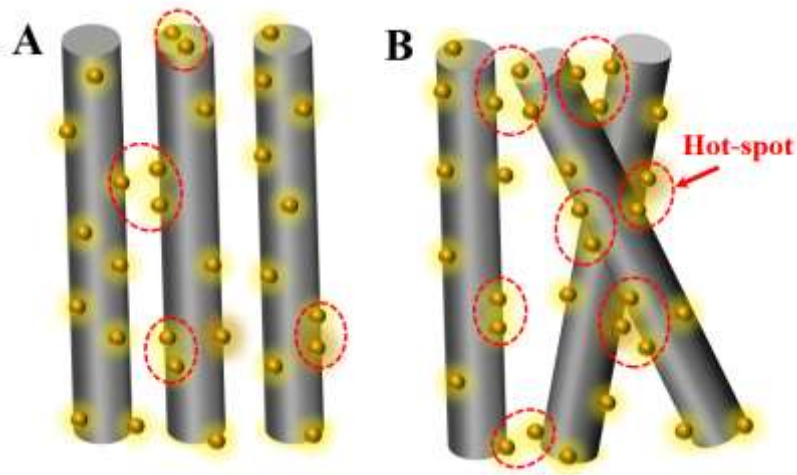

Figure S14: Schematic diagram showing the "hot-spots" phenomenon of different ZnO-Ag nanoarray patterns. (A) Vertical and parallel pattern of ZnO-Ag nanorods with limited "hot-spots" zones; (B) Tilted pattern of ZnO-Ag nanorods with an increased number of "hot-spots" for enhancing the plasmonic sensing performance.

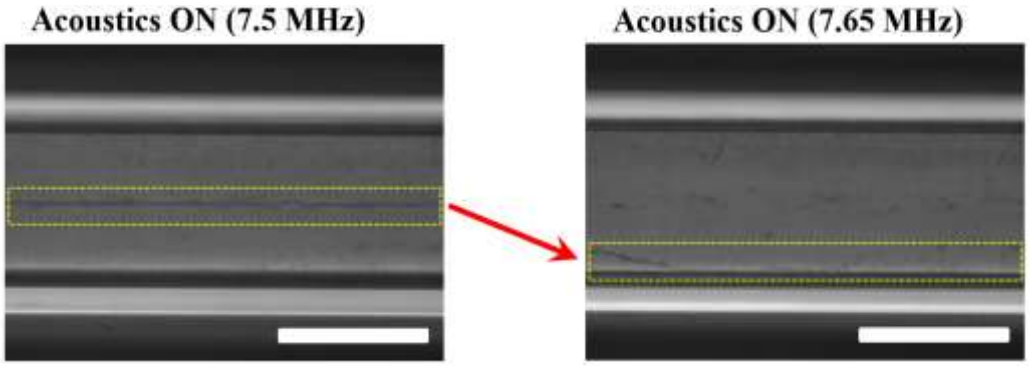

Figure S15: Top view optical images of solution with SNs-400 particles in plasmonic nanoarray-deocrated glass capillary. From the right figure, a streaking effect was shown for demonstrating the movement of nanoparticles from the middle to the edge regions.

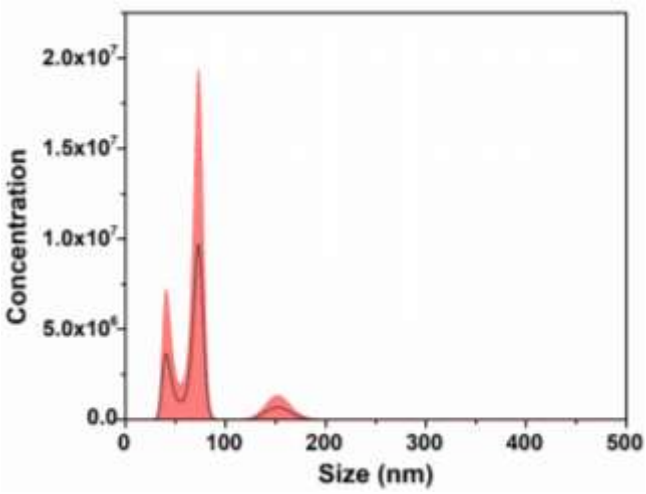

Figure S16: NTA analysis showing the size distribution profiles of ExoStd™ human urine exosomes.

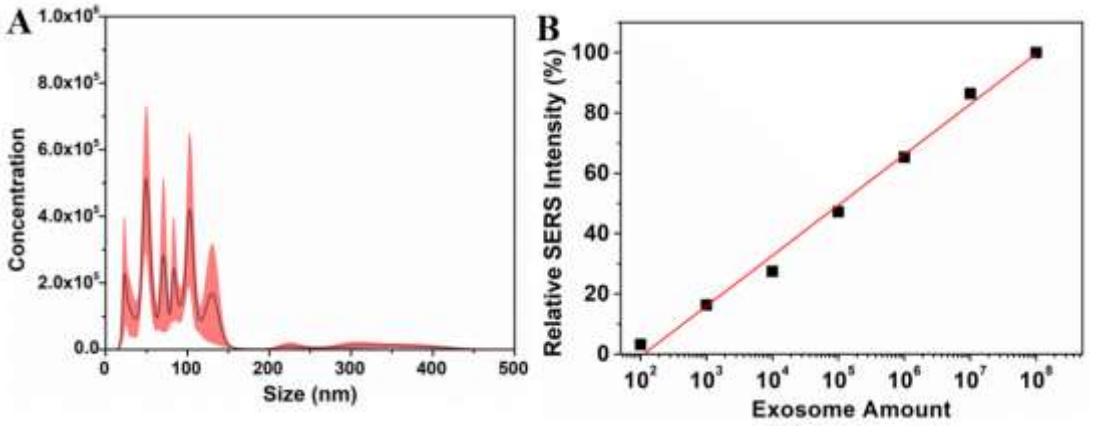

Figure S17: (A) NTA analysis human plasma-derived exosomes. The isolation of exosomes from human plasma was followed by our previously developed acoustofluidic method.[6] (B) Relative SERS intensity of exosomes-bound SNs-400 at different concentrations of exosomes and the fitted linear relationship at peak 1241 cm^{-1} (y=16.73x - 34.26, R^2=0.991).

Table S1. Comparison of methods for exosome detection.

Detection methods	Detection setup	Exosome source	Detection range	LOD	**Ref**erence
Electrochemical	Gold film	MCF-7 cells	1.12×10^{2}-1.12×10^{8} exosomes/μL	96 exosomes/μL	An et al.[7]
Electrochemical	Magnetic bead	HepG2 cells	1×10^{5}-5×10^{7} exosomes/mL	1.72×10^{4} exosomes/mL	Cao et al.[8]
Immunofluorescent	NaYF4:Yb, Er nanocrystal	HepG2 cells	1×10^{4}-1×10^{8} exosomes/μL	1.1×10^{3} exosomes/μL	Chen et al.[9]
Colorimetric	Magnetic bead	PC3 and Hela cells; plasma	0.4×10^{8}-6×10^{8} exosomes/mL	3.58×10^{6} exosomes/mL	Chen et al.[10]
Colorimetric	ZnO nanowire	MCF-7 cells; serum	2.2×10^{5}-2.4×10^{7} exosomes/μL	2.2×10^{4} exosomes/μL	Chen et al.[11]
Thermal response	Au@Pd nanopopcorn	Serum	10^{4}-10^{8} exosomes/μL	1.4×10^{4} exosomes/μL	Cheng et al.[12]
Electrochemical	Gold film	MCF-7 cells	2×10^{4}-1×10^{6} exosomes/μL	200 exosomes/μL	Doldán et al.[13]
Electrochemical	Magnetic bead	LNCaP, MCF-7, and Hela cells	1×10^{3}-1.2×10^{5} exosomes/μL	70 exosomes/μL	Dong et al.[14]
SPRi	Gold nanoparticle	NSCLC cells; plasma	3.135×10^{4}-100×10^{4} exosomes/μL	10^{4} exosomes/μL	Fan et al.[15]
Immunofluorescent	CuO nanoparticle	HepG2 cells	7.5×10^{4}-1.5×10^{7} exosomes/μL	4.8×10^{4} exosomes/μL	He et al.[16]
Colorimetric	Magnetic bead	HepG2 cells; serum	2.2×10^{4}-4.3×10^{8} exosomes/μL	2.2×10^{3} exosomes/μL	He et al.[17]
Electrochemical	Magnetic bead	MCF-7 cells; serum	1.5×10^{5}-1×10^{6} exosomes/μL	10^{5} exosomes/μL	Moura et al.[18]
SERS	Gold nanoparticle	Cell culture media (PC9, H1299, and HPAEC cells)	1×10^{9}-10×10^{9} exosomes/mL	N/A	Shin et al.[19]
Quartz crystal microbalance	Gold film	HUMSC cells	2.5×10^{8}-5×10^{10} exosomes/mL	1.4×10^{8} exosomes/mL	Suthar et al.[20]
SERS	Gold nanoparticle	MCF-7 cells	1×10^{5}-5×10^{8} exosomes/mL	5×10^{3} exosomes/mL	Wang et al.[21]
Colorimetric	Single-wall carbon nanotube	MCF-7 cells	1.84×10^{6}-2.21×10^{7} exosomes/μL	5.2×10^{5} exosomes/μL	Xia et al.[22]
Fluorescent	Sepharose CL-4B	TK-6 cells	2×10^{8}-1.5×10^{9}	2.9×10^{7}	Xu et al.[23]

			exosomes/mL	exosomes/mL	
Electrochemical	Gold nanoparticle	MCF-7 cells	5×10^{2}-5×10^{6} exosomes/μL	125 exosomes/μL	Zhang et al.[24]
Immunofluorescent	Magnetic nanoparticle in PDMS channel	Plasma	2.5×10^{6}-2.5×10^{7} exosomes/mL	7.5×10^{5} exosomes/mL	Zhao et al.[25]
Magneto-resistive	MoS_2-Fe_3O_4	A431 cells	10^{2}-10^{8} exosomes	100 exosomes	Zhu et al.[26]
Immunofluorescent	Silica nanoparticle	Human urine	10^{4}-10^{8} exosomes/μL	1.3×10^{3} exosomes/μL	This study
SERS	3D ZnO-Ag plasmonic nanoarray	Plasma	10^{2}-10^{8} exosomes/μL	20 exosomes/μL	This study

References:

[1] P. Huang, Y. Xie, D. Ahmed, J. Rufo, N. Nama, Y. Chen, C. Y. Chan, T. J. Huang, Lab Chip 2013, 13, 3847.

[2] P. Huang, S. Zhao, H. Bachman, N. Nama, Z. Li, C. Chen, S. Yang, M. Wu, S. P. Zhang, T. J. Huang, Adv. Sci. 2019, 6, 1970113.

[3] N. Hao, P. Liu, H. Bachman, Z. Pei, P. Zhang, J. Rufo, Z. Wang, S. Zhao, T. J. Huang, ACS Nano 2020, 14, 6150.

[4] N. Nama, P.-H. Huang, T. J. Huang, F. Costanzo, Biomicrofluidics 2016, 10, 024124.

[5] N. Nama, P.-H. Huang, T. J. Huang, F. Costanzo, Lab Chip 2014, 14, 2824.

[6] M. Wu, Y. Ouyang, Z. Wang, R. Zhang, P.-H. Huang, C. Chen, H. Li, P. Li, D. Quinn, M. Dao, S. Suresh, Y. Sadovsky, T. J. Huang, Proc. Natl. Acad. Sci. U.S.A. 2017, 114, 10584.

[7] Y. An, T. Jin, Y. Zhu, F. Zhang, P. He, Biosens. Bioelectron. 2019, 142, 111503.

[8] Y. Cao, L. Li, B. Han, Y. Wang, Y. Dai, J. Zhao, Biosens. Bioelectron. 2019, 141, 111397.

[9] X. Chen, J. Lan, Y. Liu, L. Li, L. Yan, Y. Xia, F. Wu, C. Li, S. Li, J. Chen, Biosens. Bioelectron. 2018, 102, 582.

[10] J. Chen, Y. Xu, Y. Lu, W. Xing, Anal. Chem. 2018, 90, 14207.

[11] Z. Chen, S.-B. Cheng, P. Cao, Q.-F. Qiu, Y. Chen, M. Xie, Y. Xu, W.-H. Huang, Biosens. Bioelectron. 2018, 122, 211.

[12] N. Cheng, Y. Song, Q. Shi, D. Du, D. Liu, Y. Luo, W. Xu, Y. Lin, Anal. Chem. 2019, 91, 13986.

[13] X. Doldán, P. Fagúndez, A. Cayota, J. Laíz, J. P. Tosar, Anal. Chem. 2016, 88, 10466.

[14] H. Dong, H. Chen, J. Jiang, H. Zhang, C. Cai, Q. Shen, Anal. Chem. 2018, 90, 4507.

[15] Y. Fan, X. Duan, M. Zhao, X. Wei, J. Wu, W. Chen, P. Liu, W. Cheng, Q. Cheng, S. Ding, Biosens. Bioelectron. 2020, 154, 112066.

[16] F. He, J. Wang, B.-C. Yin, B.-C. Ye, Anal. Chem. 2018, 90, 8072.

[17] F. He, H. Liu, X. Guo, B.-C. Yin, B.-C. Ye, Anal. Chem. 2017, 89, 12968.

[18] S. L. Moura, C. G. Martín, M. Martí, M. I. Pividori, Biosens. Bioelectron. 2020, 150, 111882.

[19] H. Shin, H. Jeong, J. Park, S. Hong, Y. Choi, ACS Sens. 2018, 3, 2637.

[20] J. Suthar, E. S. Parsons, B. W. Hoogenboom, G. R. Williams, S. Guldin, Anal. Chem. 2020, 92, 4082.

[21] Q. Wang, L. Zou, X. Yang, X. Liu, W. Nie, Y. Zheng, Q. Cheng, K. Wang, Biosens. Bioelectron. 2019, 135, 129.

[22] Y. Xia, M. Liu, L. Wang, A. Yan, W. He, M. Chen, J. Lan, J. Xu, L. Guan, J. Chen, Biosens. Bioelectron. 2017, 92, 8.

[23] R. Xu, A. Fitts, X. Li, J. Fernandes, R. Pochampally, J. Mao, Y.-M. Liu, Anal. Chem. 2016, 88, 10390.

[24] H. Zhang, Z. Wang, Q. Zhang, F. Wang, Y. Liu, Biosens. Bioelectron. 2019, 124–125, 184.

[25] Z. Zhao, Y. Yang, Y. Zeng, M. He, Lab Chip 2016, 16, 489.

[26] F. Zhu, D. Li, Q. Ding, C. Lei, L. Ren, X. Ding, X. Sun, Biosens. Bioelectron. 2020, 147, 111787.